FLUCTUATIONS IN THE WISCONSIN TOROIDAL OCTUPOLE

J.A. Schmidt, D.E. Lencioni, and J.C. Sprott

July
1967

PLP 132

University of Wisconsin
Thermonuclear Plasma Studies

FLUCTUATIONS IN THE WISCONSIN TOROIDAL OCTUPOLE

(Presented at the June 1967 Princeton Meeting of the International Symposium on Fluctuations and Diffusion in Plasmas)

J. A. Schmidt, D. E. Lencioni, J. C. Sprott

Measurements have been made and reported concerning the injection, transport and quiescent periods in the toroidal octupole. The opportunity is now open to study in greater detail the loss of plasma to walls and rod supports.

Figure 1 shows the experimental apparatus. A conical pinch gun injects a hydrogen plasma through collimating slots into a toroidal octupole field. After the filling process taking ~ 100 μsec the central body of the plasma becomes quiescent. The initial quiescent plasma has a maxwellian ion energy distribution of approximately 40 eV with 10eV electrons, the maximum density at early times is of the order of $10^{10} P/cm^3$. The plasma is then lost to the rod supports since they intersect all flux shells, as well as to the walls by diffusion across field lines.

The magnetic field is created by currents flowing in four rods along with image currents flowing in the tank walls. The currents are induced by an iron core threaded through

the toroid.

The time variation of the magnetic field is sinisodial, with a half period of 5 msec. The times during which measurements were made were near the peak of the field.

Figure 2 shows a plot of the intersection of the constant surfaces of the flux function ψ with a cross section of the octupole. The lines shown are also the magnetic field lines. The boundary of hydromagnetic stability, i.e., the surface at which the volume of flux tubes begins to increase moving outward from the separatrix is labeled ψ_c. If the plasma pressure decreases monotonically moving away from the separatrix toward the rods or wall, the plasma would be hydromagnetically stable except for a region outside ψ_c along the wall. Note the numerical labeling of the flux surfaces.

We look first at fluctuations <u>outside</u> the separatrix where during the experimental times the density decreases monotonically toward the walls.

Potential fluctuation of the order of 4 volts appear outside ψ_c. The fluctuations amplitude decreases monotonically toward the separatrix, inside ψ_c.

Figure 3 shows the fluctuations in potential in the

unstable region. The oscillograph was taken 2 cm from the wall on the horizontal midplane. Note the injection period. The fluctuations have a wavelength of about 3 cm and an excellent connection along field lines.

The fluctuations have a maximum amplitude of about 4 volts and decay in about 800 μsec. The fluctuations inside ψ_c are smaller in amplitude but die away with the same rate.

A reason for the decrease in fluctuations with time can be derived from the density distribution in this region, shown in Figure 4. The density in this region is of the order of a few x $10^8/cm^3$. ψ_c appears at approximately 2.5 cm from the wall. Shortly after injection a density gradient exists in the unstable region outside ψ_c, which drives the instabilities in this region. As time passes the density flattens in the unstable region as shown by the density distributions at successively later times. The density gradient is supported inside ψ_c in the flute stable region after the fluctuations have evolved the distribution. When the density gradient is removed at approximately 800 μsec in the unstable region the fluctuations disappear as seen in the Figure 3.

If a containment device has an unstable region which

shakes the adjoining stable regions and thereby increases the plasma loss in both it is apparent from these measurements that the losses will be reduced when the density distribution has evolved to limit the driving mechanism for the fluctuations.

The flattening of the density outside ψ_c leaving the density gradients to be supported by flux surfaces inside the ψ_c, illustrates the fact that the diffusion coefficient in the inner regions is much smaller than in the unstable regions outside ψ_c.

It is of interest to determine the autocorrelation function as well as the frequency spectra of the fluctuations. A circuit does not suffice to determine the autocorrelation function directly due to the short sampling time provided. A sample of the fluctuating electric field can be obtained by using several appropriately delayed oscilloscopes. The data can then be read at successive intervals and the resulting digitized data can be fed into a computer to determine the autocorrelation function.

The autocorrelation function from several samples can be averaged together to give good convergence. A 1 meg ohm input impedence attenuated electric field probe was used. An 80 μsec long sample was taken 200 μsec after injection. The

sample comprised 4 oscillographs.

Figure 5 shows the autocorrelation for a fluctuation in the unstable region near the wall. As would be expected the fluctuations appear to be traveling waves which become uncorrelated rapidly in time. After a few cycles the fluctuations lose most of their correlation.

It is interesting to note that the diffusion coefficient calculated as shown in Figure 6 by integrating the correlation function over its time argument gives a value close to Bohm.

$$D = \frac{1}{B^2} \int_0^\infty C(\tau)\, d\tau$$

$$D = \frac{2\pi \langle \delta n \, \delta V \rangle}{\lambda_\perp B \nabla n}$$

Fig. 6

This value was also obtained previously by measuring $\delta V + \delta n$ using the last equation in this figure.

The approximate power spectra can be obtained by

matching the autocorrelation to an analytic function. Since the match is only approximate, the exact form and fine details of the spectra will not be correct but the central frequency will be quite accurate and a good measure of the band width will also be obtained. Figure 7 shows the power spectra obtained from this correlation function. Note the broad spectra of frequencies present. The full width at half maximum is about 50 kHz. The main frequency component is about 80 kHz.

We move now to flux surfaces inside the separatrix toward the rods. The density gradient does not decrease everywhere moving away from the separatrix toward the rods. During injection the largest density is deposited under the rods slightly off the separatrix. Figure 8 shows this density gradient. The energy required to interchange flux tubes in this region can be calculated and shows marginal stability, yet fluctuations are observed as seen in this figure.

Even though large fluctuations exist here the density gradient persists to late times. The flattening observed near the wall does not take place here.

The fluctuations are fairly sinosoidal; they have maximum amplitude of 3 volts and a wavelength of approximately 6 cm. They are found under all four rods in a fairly limited region.

The correlation function for these fluctuations can be determined in the same manner as those outside ψ_c, and appears in Figure 9. Contrasting this autocorrelation function with the one found outside ψ_c, the frequency is about 250 kHz compared to 80 kHz outside ψ_c.

The correlation time for these fluctuations is very much longer than the correlation time for the more random fluctuations outside ψ_c. These fluctuations go through 10 or more cycles without losing appreciable correlation.

The power spectra can be derived from this correlation function and is shown in Figure 10. The peak is centered at 250 kHz with a half width of 7 kHz. The spectra is expanded 100 times near zero frequency to illustrate the sharpness of the spectra. The peak power density is about twice that of the fluctuations outside ψ_c although the total power is less due to the small band width. The diffusion coefficient can be estimated for this region by integrating the autocorrelation function. The diffusion coefficient so derived is two orders of magnitude below Bohm due to the excellent time correlation of the fluctuations. The relatively small diffusion coefficient explains the fact that an inverse density gradient persists in this region.

The diffusion coefficient for the fluctuations near the wall has been measured and reported previously by Meade. The determination was accomplished by simultaneous measurements of the potential and density fluctuations. The results are shown in Figure 11 for the horizontal midplane. The Bohm diffusion coefficient is also shown for comparison.

The observed coefficient approaches the Bohm level outside the stable region although dropping next to the wall due to the walls shorting of the electric fields. The observed diffusion coefficient drops rapidly upon entering the stable region to a value four orders of magnitude less than Bohm a few cm inside of ψ_c on the midplane.

It is of interest to know if the observed diffusion coefficient along with hanger losses can be used to predict quantitatively the observed plasma lifetime. It is also of interest to know what lifetime would be expected if pumpout at the Bohm rate were to occur in the octupole. To determine these aspects for the octupole, the plasma diffusion and hanger loss were simulated on a computer. The first simulation was made with the observed diffusion coefficient neglecting any hanger losses. The observed density distribution at 500 μsec was fed into the computer and the density evolution

simulated for the next 500 μsec.

The evolution is shown in Figure 12. The initial density distribution at 500 μsec is shown along with the evolved distribution at 1000 μsec. There is no large loss of plasma to the walls during these times only a redistribution to regions nearer the walls. No growth in density in these regions is observed in the actual experiment. The predicted lifetime from this evolution is quite long, much longer than observed in the actual experiment. These facts illustrate that the rod supports must be important in determining the density evolution.

A support loss was added in the next calculation. The loss to each flux shell was proportional to the area of intersection of the flux shells with the supports. The resulting density evolution is shown in Figure 13. The same initial density distribution was used as in the previous calculation and the resulting evolution at 1000 μsec was determined.

The density decay is much more rapid than if support losses are neglected. A larger number of particles are lost during this time from the containment zones. A small inversion of density is predicted, and a general flatting of density can be noted. The lifetime as well as the detailed

density evolution agrees quite well with those observed in the actual experiment.

It was found that if a density distribution other than the observed one was used as the starting point, the observed distribution did not evolve in a reasonable time interval. The distribution of density at late times appears then to be a strong function of the injection and filling processes. Figure 14 illustrates the evolution assuming a diffusion coefficient of the Bohm value throughout the octupole along with losses due to rod supports.

For this case the density decays very rapidly into a distribution not observed in the actual experiment with a lifetime 15 times shorter than observed in the octupole.

If the evolution during the intervening time intervals between the two curved here are observed a normal mode is seen to develop rapidly which was quite independent of the initial distribution.

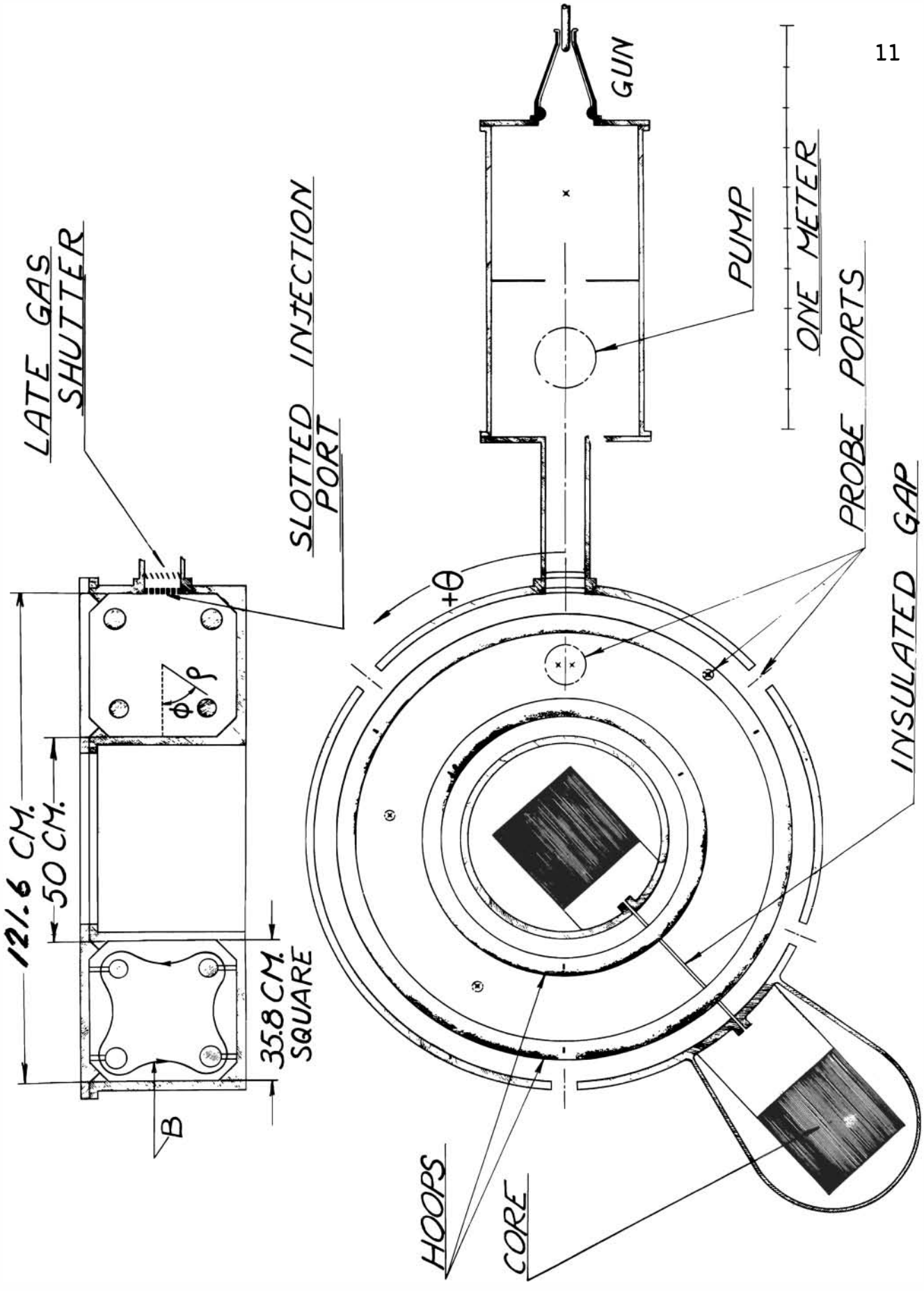
LATE GAS SHUTTER
SLOTTED INJECTION PORT
GUN
PUMP
ONE METER
PROBE PORTS
INSULATED GAP
+θ
121.6 CM.
50 CM.
35.8 CM. SQUARE
B
HOOPS
CORE

Figure 1

θ = CONST. PLANE: FLUX PLOT

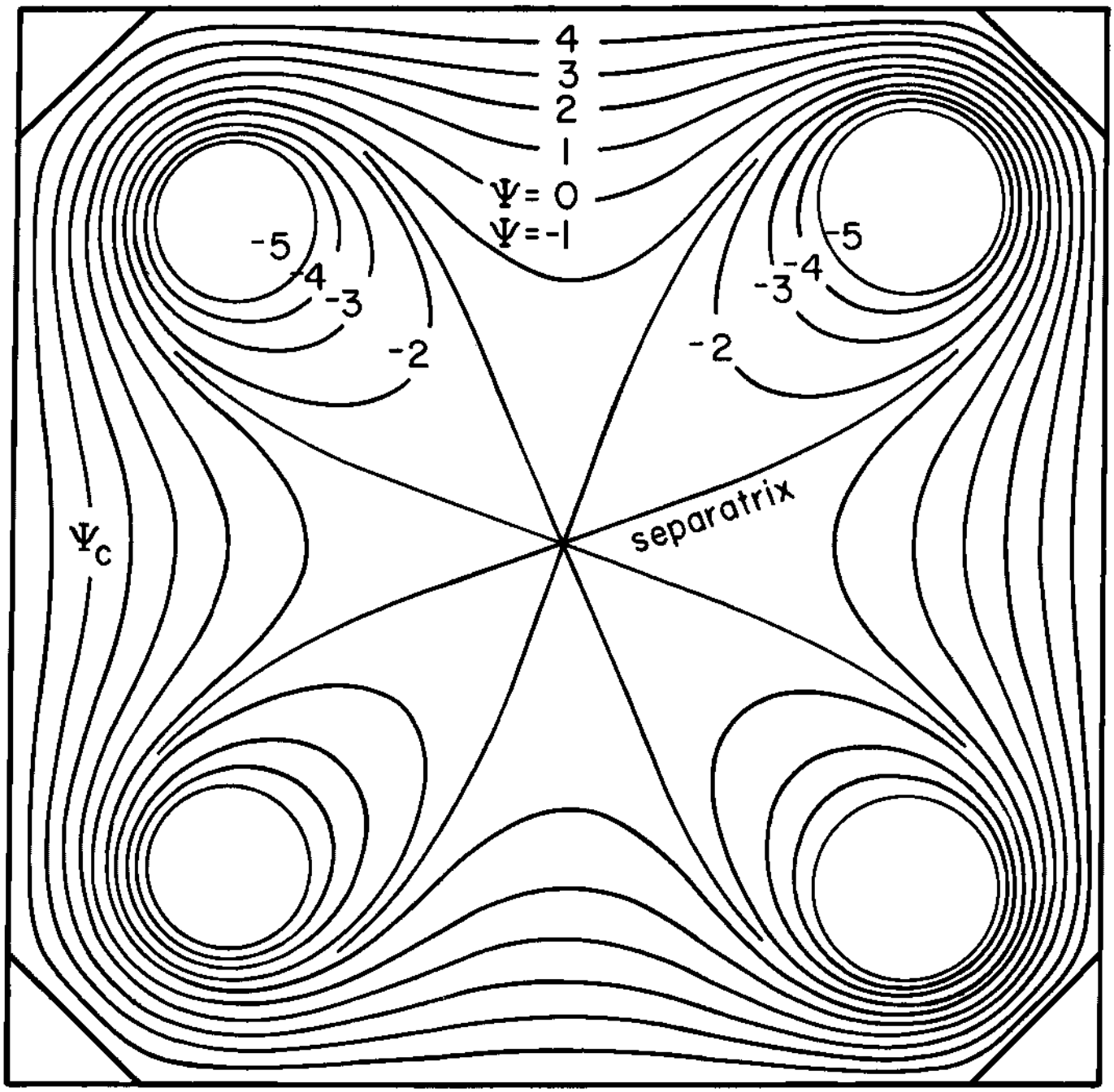

Figure 2

Floating Potential Fluctuations

2 cm From Wall

V_f

2.7 volts / Div.

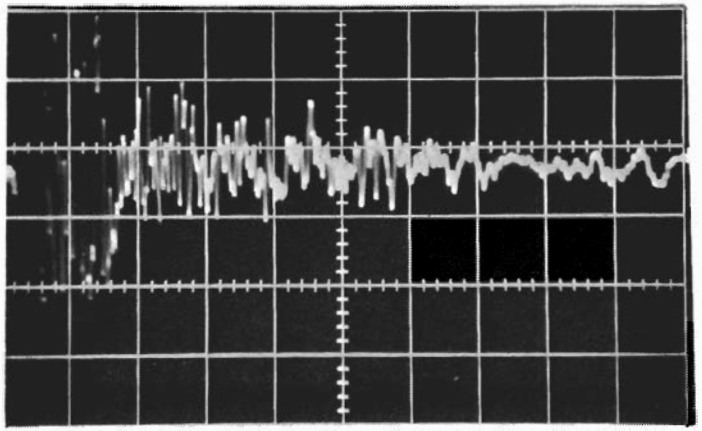

Time

100 μ Sec. / Div.

Figure 3

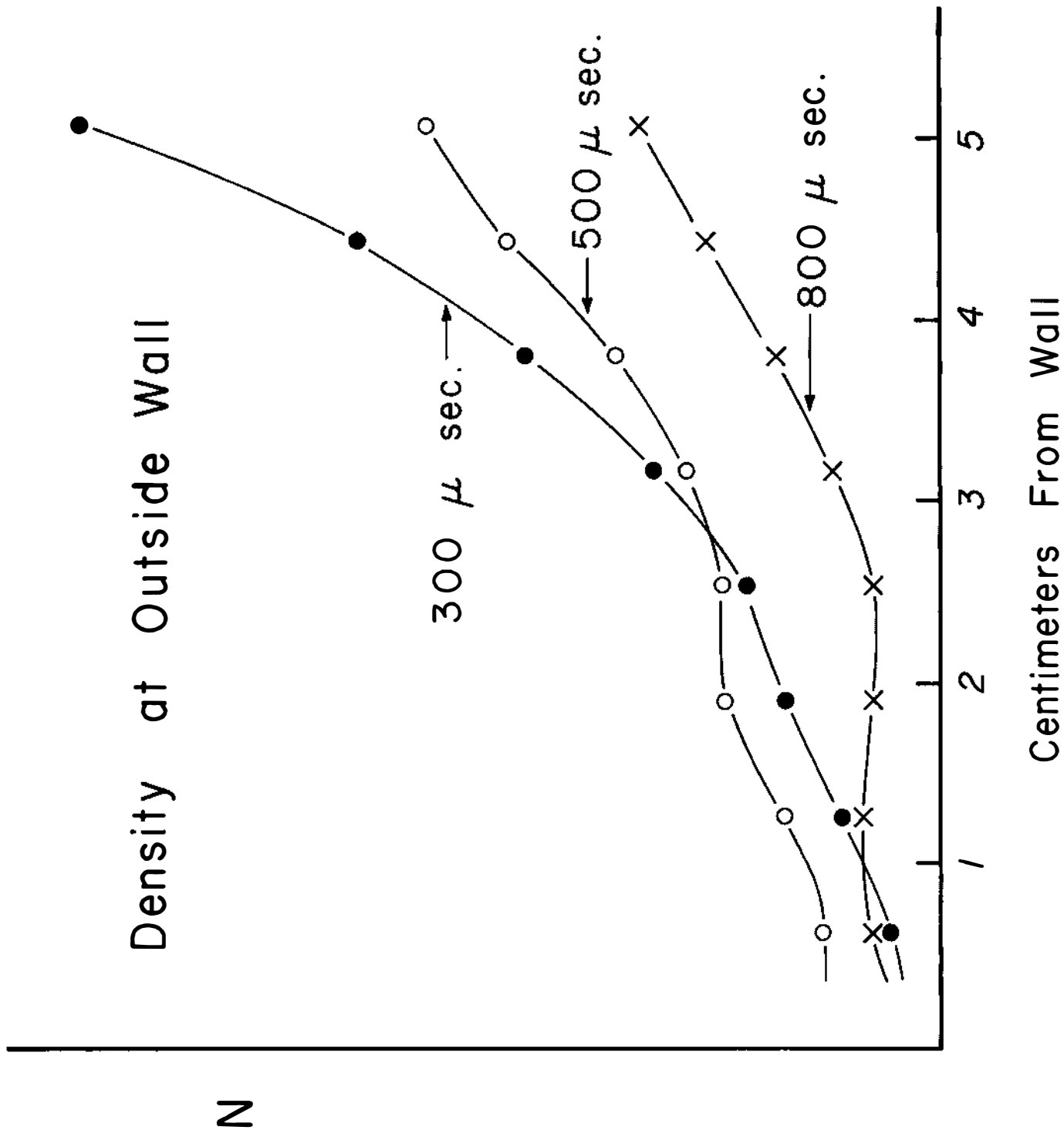
N
Density at Outside Wall
300 μ sec.
500 μ sec.
800 μ sec.
1
2
3
4
5
Centimeters From Wall

Figure 4

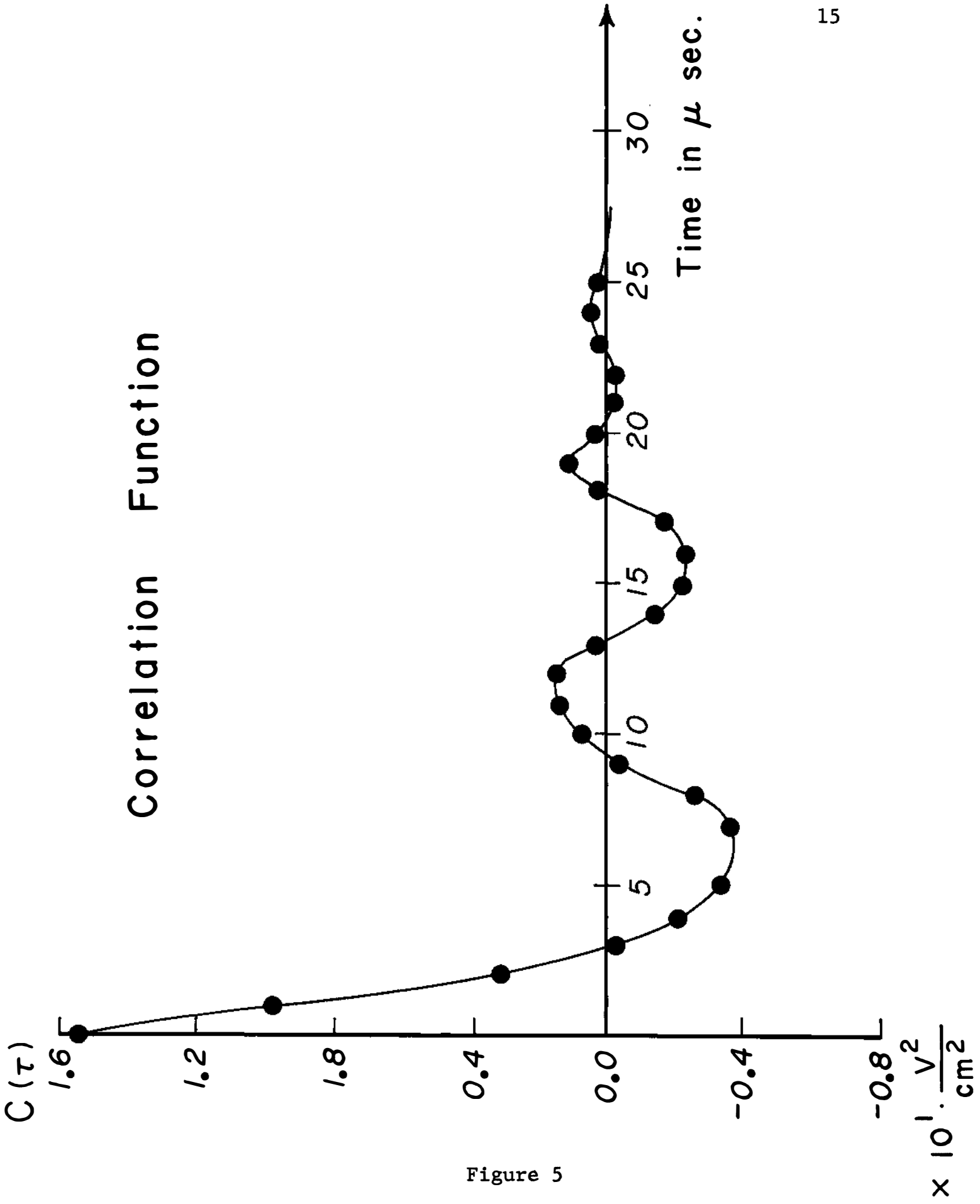
Correlation Function
C(τ)
1.6
1.2
0.8
0.4
0.0
-0.4
-0.8
× 10¹ · V²/cm²
5
10
15
20
25
30
Time in μ sec.

Figure 5

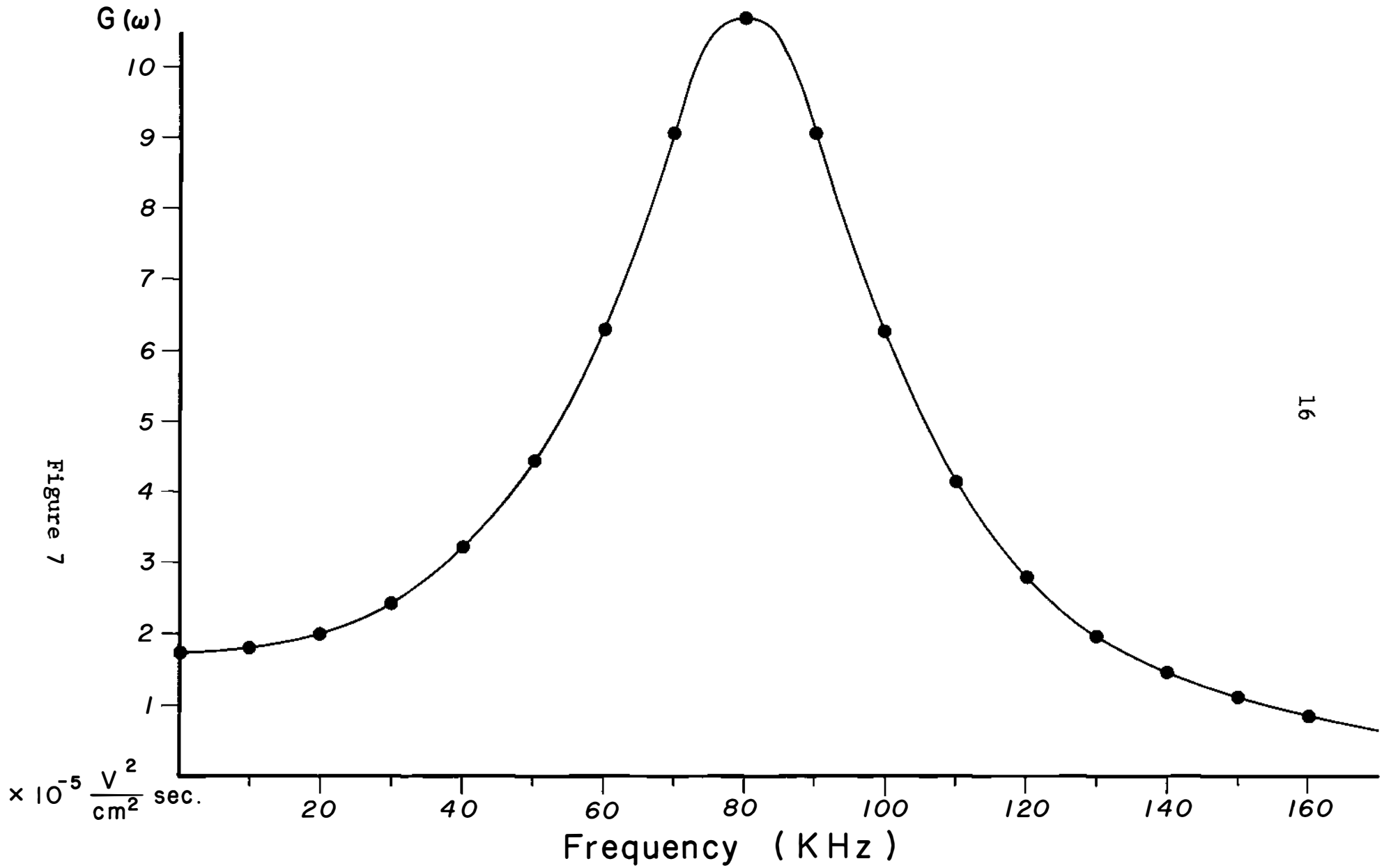
POWER SPECTRA
G (ω)
10
9
8
7
6
5
4
3
2
1
× 10⁻⁵ V²/cm² sec.
20
40
60
80
100
120
140
160
Frequency (KHz)

Figure 7

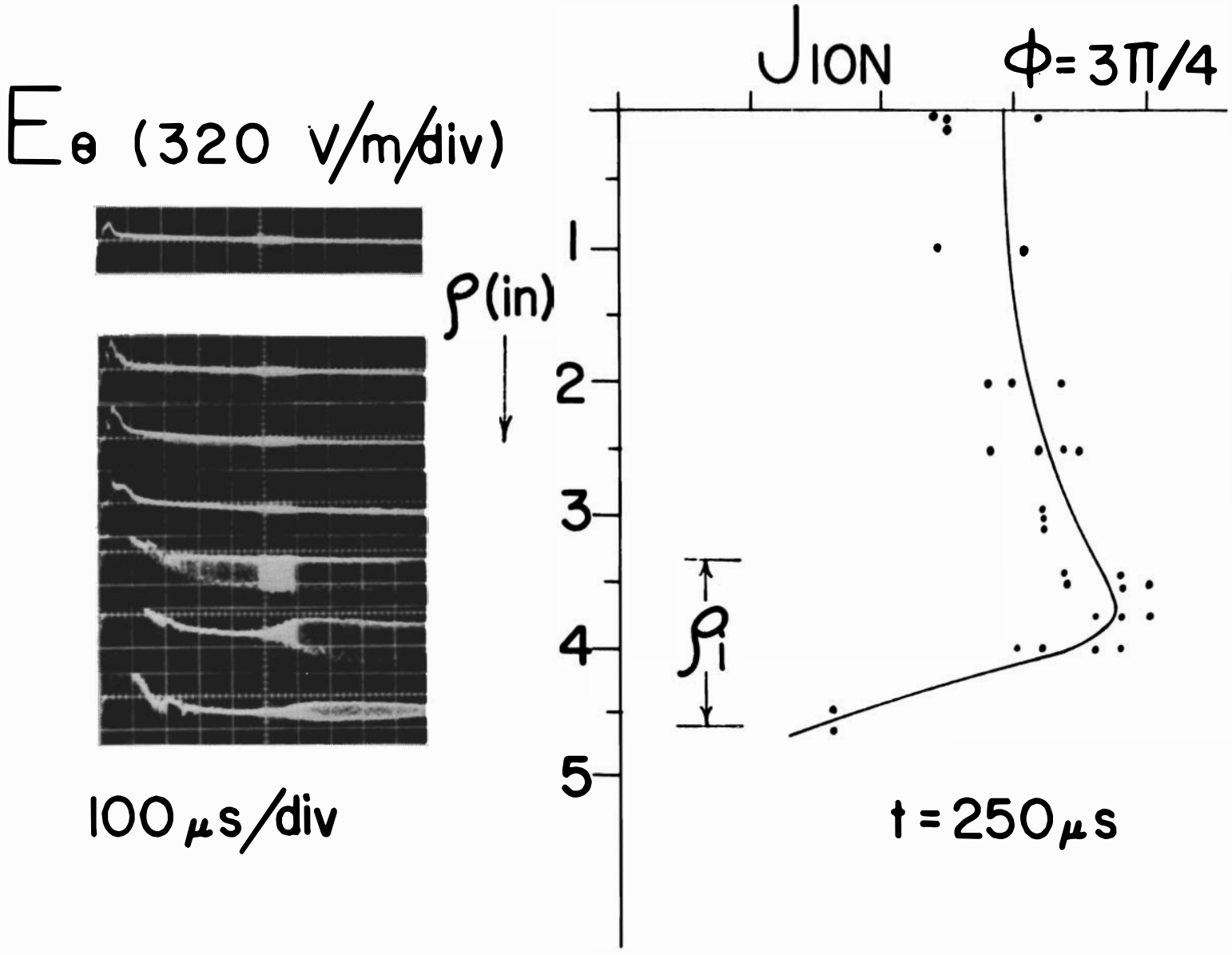

Figure 8

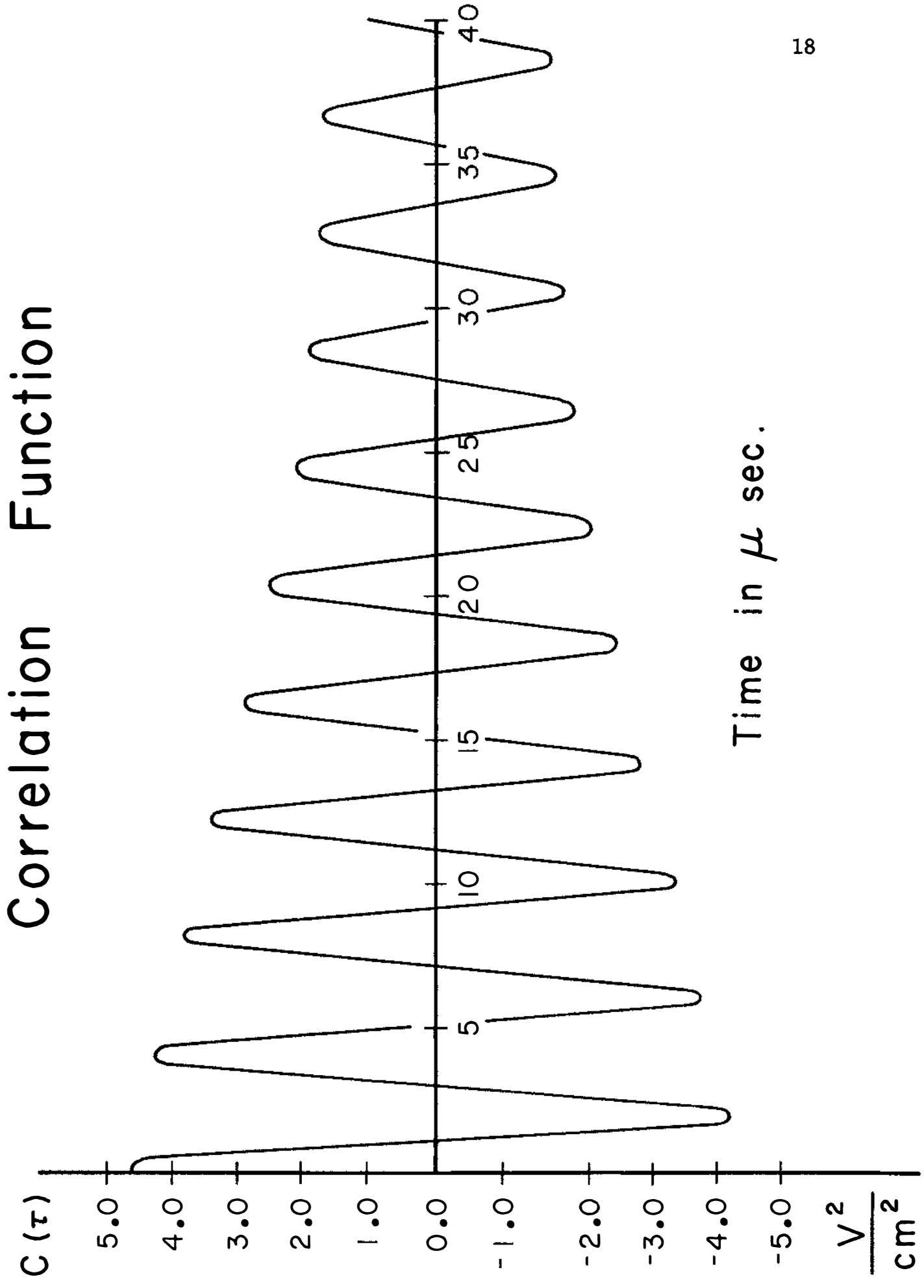
Correlation Function
C(τ)
5.0
4.0
3.0
2.0
1.0
0.0
-1.0
-2.0
-3.0
-4.0
-5.0
V²/cm²
5
10
15
20
25
30
35
40
Time in μ sec.

Figure 9

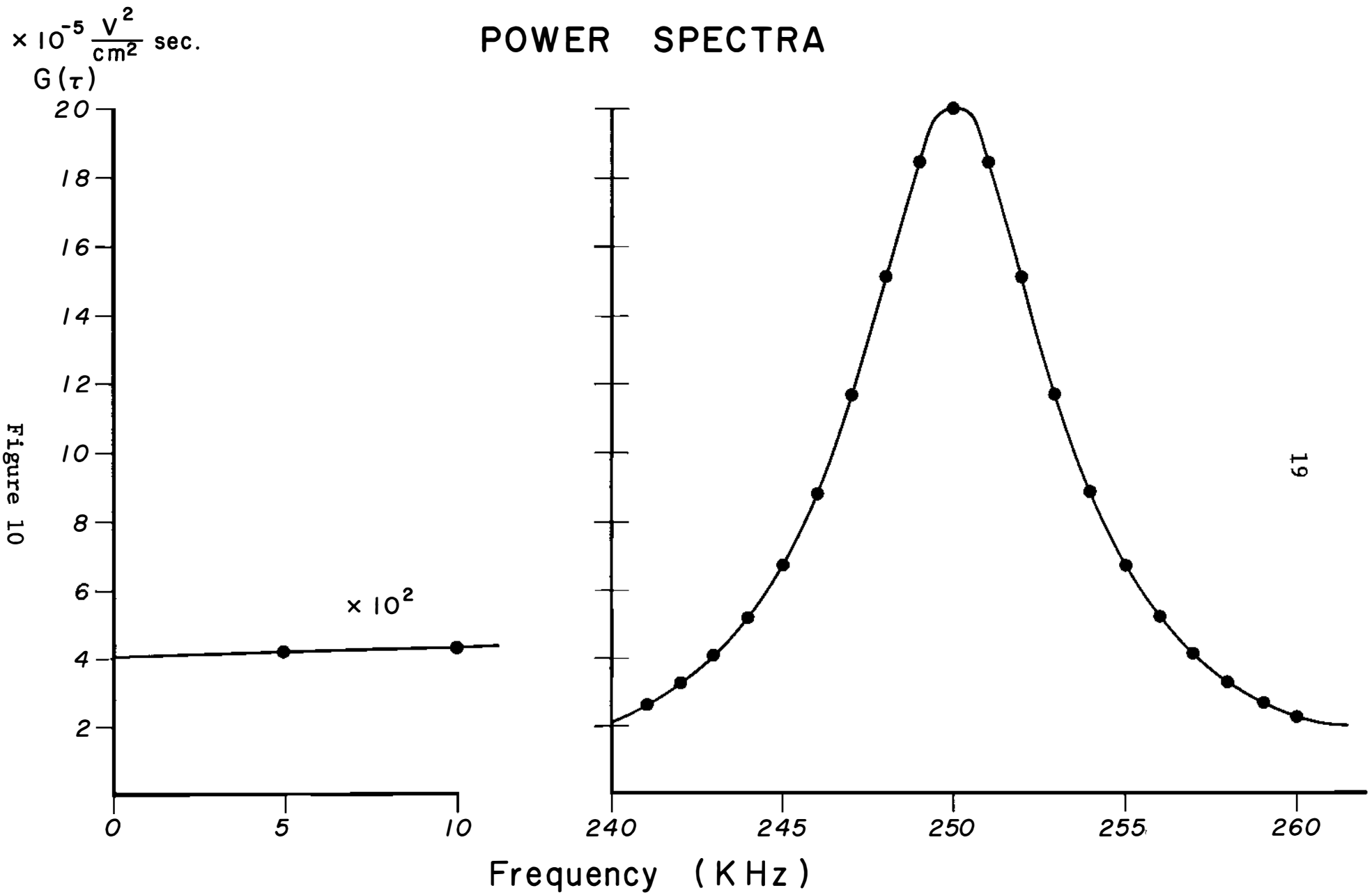
POWER SPECTRA
× 10⁻⁵ V²/cm² sec.
G(τ)
20
18
16
14
12
10
8
6
4
2
× 10²
0
5
10
240
245
250
255
260
Frequency (KHz)

Figure 10

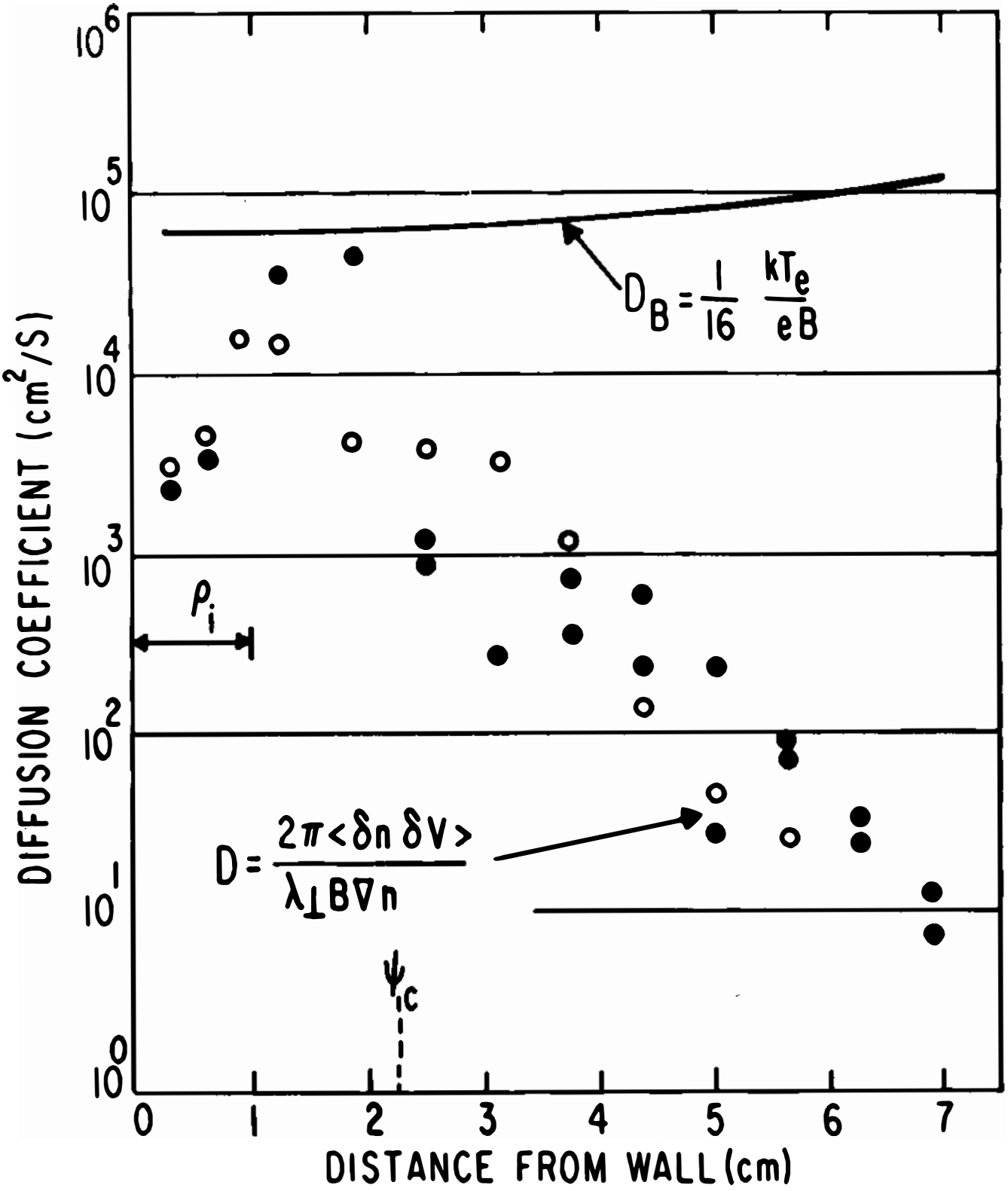
DIFFUSION COEFFICIENT (cm²/S)
10⁶
10⁵
10⁴
10³
10²
10¹
10⁰
D_B = 1/16 kT_e/eB
ρ_i
D = 2π<δn δV> / λ⊥B∇n
ψ_c
0
1
2
3
4
5
6
7
DISTANCE FROM WALL (cm)

Figure 11

Density Evolution Without Hangers

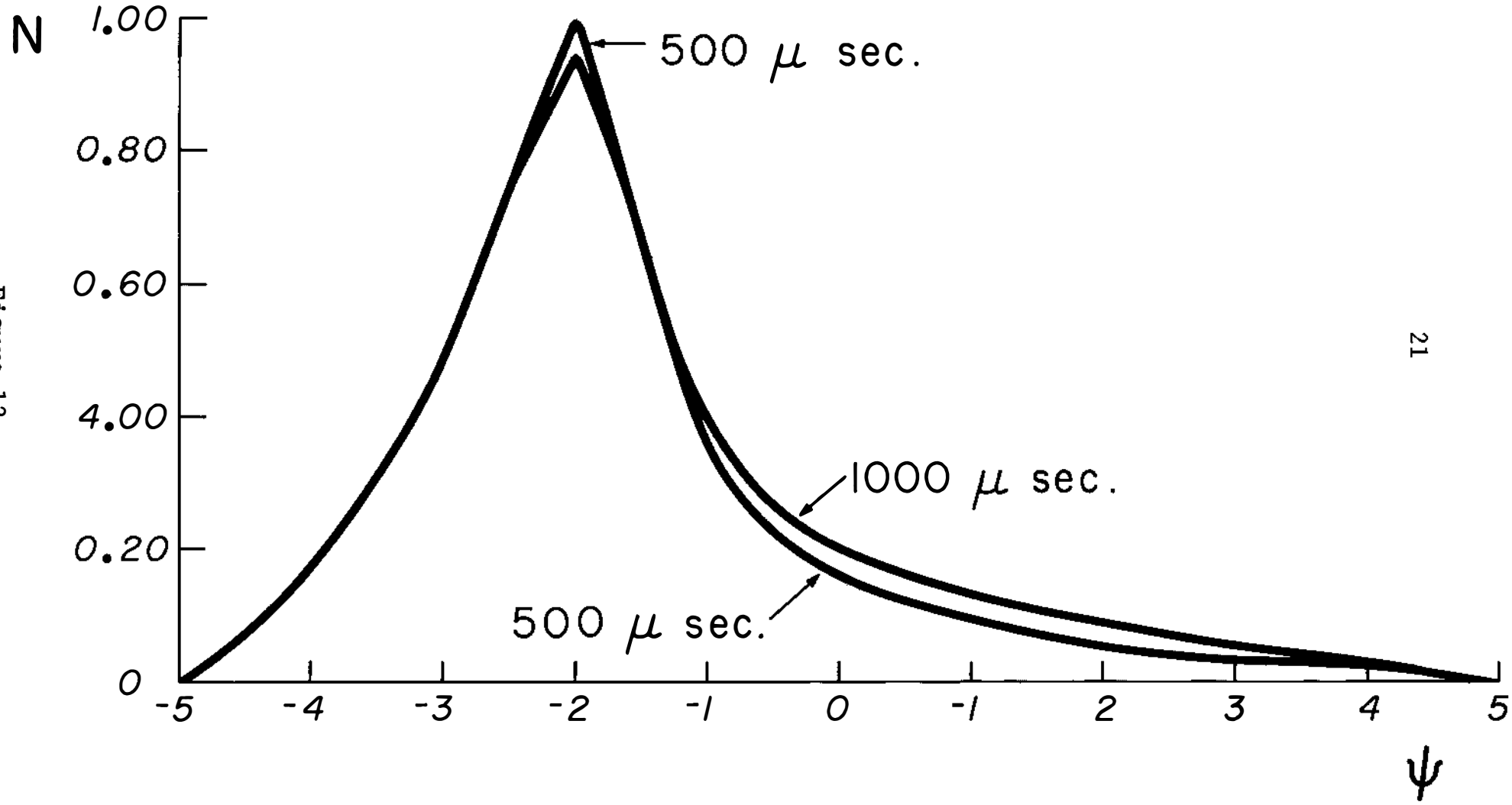

Figure 12

Density Evolution With Hangers and Observed Diffusion Coefficient

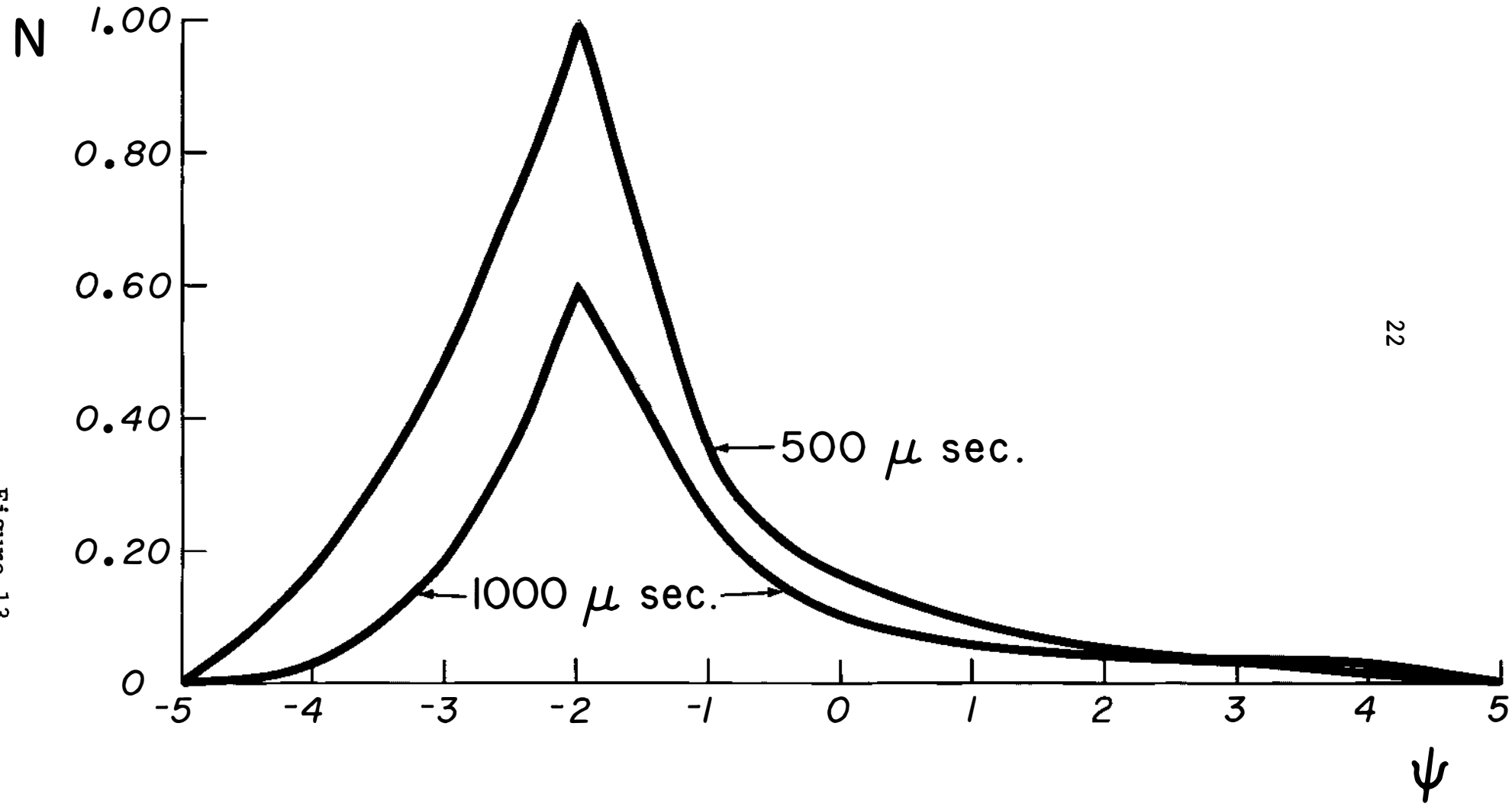

Figure 13

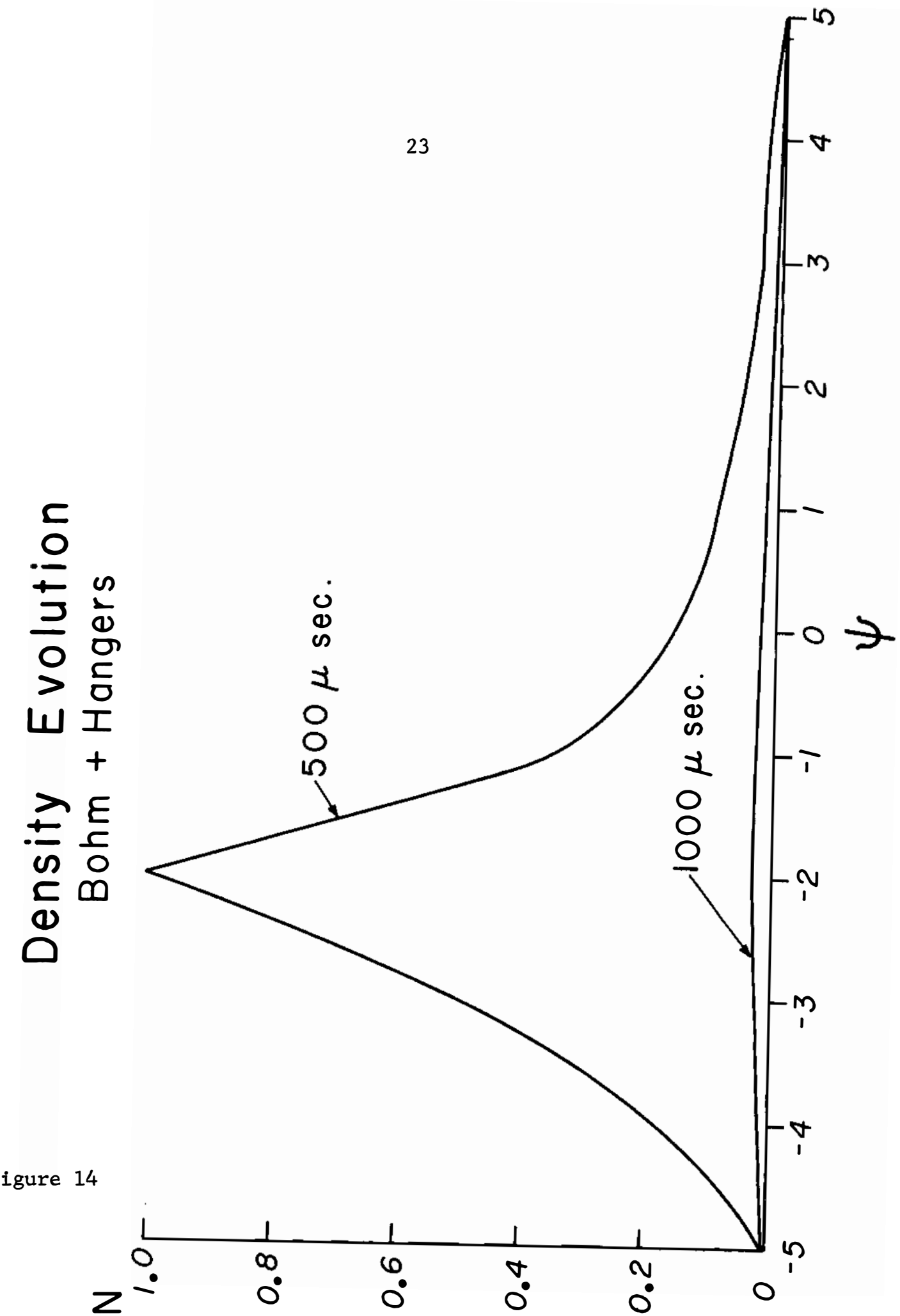
Density Evolution
Bohm + Hangers
500 μ sec.
1000 μ sec.
N
1.0
0.8
0.6
0.4
0.2
0
5
4
3
2
1
0
-1
-2
-3
-4
-5
ψ

Figure 14

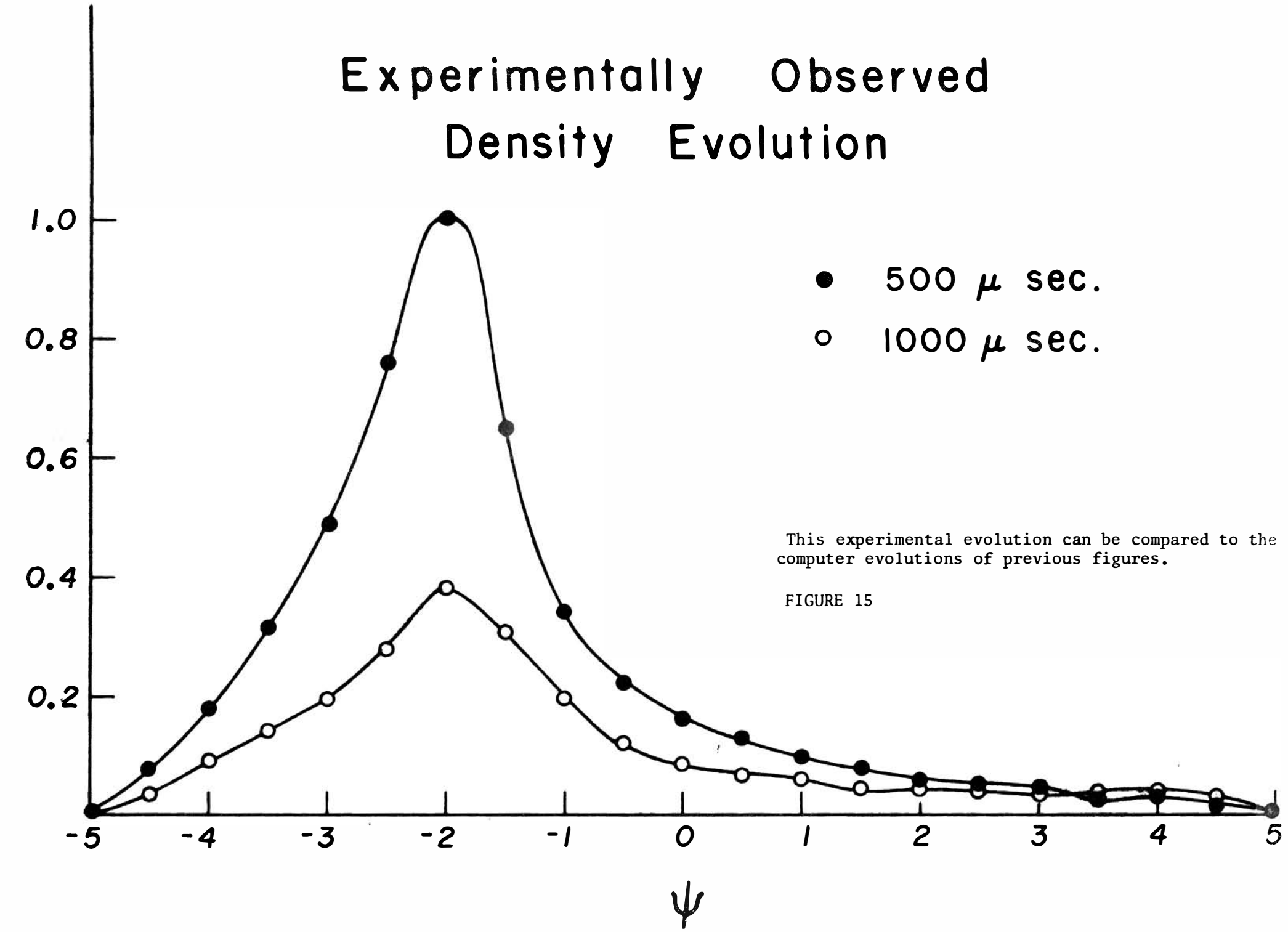

This experimental evolution can be compared to the computer evolutions of previous figures.

FIGURE 15